

Article

Rapid Process Natural Bamboo into Outdoor Bamboo-Fiber-Reinforced Composite with High Surface Photostability

Fei Rao ^{1,2,*}, Yaohui Ji ³, Yang Yang ^{4,5}, Yahui Zhang ³, Neng Li ^{2,*}, Wenji Yu ³ and Yuhe Chen ²

- ¹ Department of Industrial Design, School of Art and Design, Zhejiang Sci-Tech University, No. 2 Street 928, Hangzhou 310018, China
- ² China National Bamboo Research Center, Department of Efficient Utilization of Bamboo and Wood, Wenyi Road 310, Hangzhou 310012, China; yuhec@sina.com
- ³ Department of Wood-Based Panels and Adhesives, Research Institute of Wood Industry, Chinese Academy of Forestry, Xiangshan Road, Haidian, Beijing 100091, China; jiyahui1994@gmail.com (Y.J.); zhangyhcaf@163.com (Y.Z.); chinayuwj@126.com (W.Y.)
- ⁴ College of Furniture and Art Design, Central South University of Forestry and Technology, Changsha 410000, China; loneyanzi1990@163.com
- ⁵ Green Furniture Engineering Technology Research Center, National Forestry and Grassland Administration, Changsha 410000, China
- * Correspondence: raofei@zstu.edu.cn (F.R.); lineng8657@sina.com (N.L.)

Abstract: Surface photostability strongly influences the usefulness of bamboo and bamboo-based polymer composites in outdoor environments. In this study, accelerated aging tests were conducted to investigate how UV irradiation affects the color, surface appearance, and chemical characteristics of outdoor bamboo-fiber-reinforced composite (OBFRC) prepared from moso bamboo (*Phyllostachys pubescens* Mazel) by a three-step process involving phenol-formaldehyde (PF) resin impregnation. The surface color of natural bamboo (NB) changes rapidly during irradiation, but that of OBFRC remains relatively stable: densification mitigates the negative effects of UV irradiation. More generally, OBFRC exhibits enhanced surface photostability caused by structural and chemical modifications.

Keywords: natural bamboo; outdoor bamboo-fiber-reinforced composite; surface photostability; lignin photodegradation; PF resin



Citation: Rao, F.; Ji, Y.; Yang, Y.; Zhang, Y.; Li, N.; Yu, W.; Chen, Y. Rapid Process Natural Bamboo into Outdoor Bamboo-Fiber-Reinforced Composite with High Surface Photostability. *Forests* **2021**, *12*, 446. <https://doi.org/10.3390/f12040446>

Academic Editor: Joana Ferreira

Received: 10 March 2021

Accepted: 30 March 2021

Published: 7 April 2021

Publisher's Note: MDPI stays neutral with regard to jurisdictional claims in published maps and institutional affiliations.



Copyright: © 2021 by the authors. Licensee MDPI, Basel, Switzerland. This article is an open access article distributed under the terms and conditions of the Creative Commons Attribution (CC BY) license (<https://creativecommons.org/licenses/by/4.0/>).

1. Introduction

Moso bamboo (*Phyllostachys pubescens* Mazel) contains a naturally occurring polymeric composite composed of cellulose (approximately 55%), hemicellulose (approximately 20%), and lignin (approximately 25%). In China, bamboo is a popular material for the construction of buildings, furniture, floors, and façade systems because of its elegant surface texture, attractive natural color, and comfortable finish. The application of moso-bamboo products has expanded from indoor use in furniture, flooring, utensils, and crafts, to outdoor use in public facilities, construction, and decoration [1]. However, in the outdoor environment, high energy ($75 \leq E \leq 100$ kcal/mol) components of sunlight in the ultraviolet (UV) wavelength range ($286 \leq \lambda \leq 380$ nm) can induce aging, causing surface-oxidation degradation and discoloration. Of the molecular components of bamboo, lignin is the most sensitive to UV light [2], which acts on the phenolic hydroxyl group of lignin to form free radicals. These free radicals are subsequently transformed into unsaturated carbonyl compounds (*o*- and *p*-quinonoid structures) by demethylation or side chain cleavage [3], thus causing surface yellowing of the bamboo [2]. Although hemicellulose [4] and cellulose [5] are less affected by UV than lignin, they should not be neglected: moisture from rain, dew, and snow can cause bamboo cells to swell, revealing

cell wall areas that are usually difficult to illuminate. This accelerates the photodegradation process [6] and encourages fungal erosion [4]. The combined effect of these environmental factors ultimately weakens the mechanical stability of bamboo products [7,8], reducing their surface service quality [9] and outdoor service lifetime [10,11].

Over the years, several technologies, including the use of UV stabilizers, surface treatments, and coatings, have been proven to mitigate the adverse effects of the outdoor environment. It has been demonstrated that the inclusion of organic UV absorbers in waterborne exterior coatings, such as silica-coated zinc oxide and doped titanium dioxide nanoparticles, significantly improves UV shielding performance [12]. For instance, rutile nano-TiO₂ enhances the weatherability of bamboo-fiber/high-density-polyethylene composites by retarding their photooxidation and enhancing their thermal stability [8]. The application of clear coatings containing a combination of organic/inorganic UV absorbers has been demonstrated to be effective in inhibiting the surface photodegradation of bamboo, while preserving its aesthetic characteristics as much as possible [13]. Acrylic-based coatings that have a combination of benzotriazole and zinc-oxide nanoparticles in a 2:1 ratio demonstrate the best photostabilizing efficiency among these coatings [14]. Heat-treated bamboo has better color stability during UV radiation than untreated material; however, because its chemical composition is unmodified, its photochemical performance is similar to that of untreated bamboo. The effect of heat-treatment on aging is therefore limited [15]. Similarly, acetylation treatment does not provide wood with long-lasting photoprotection [16], and the limited concentration of phenol-formaldehyde (PF) resin in the structure does not prevent lignin from being photodegraded. Hence, to ensure the durability of a module over the entire service lifetime of natural bamboo (NB), better stabilization technologies are being investigated.

To expand the applicability of bamboo to outdoor decoration and buildings, more attention should be paid to its surface photostability. Increasing the concentration of PF in its structure or adding water-soluble hindered amine light stabilizer has been shown to improve the photoprotection efficiency of wood [6]. Hence, in this study, a simple three-step method is employed, consisting of mechanical fluffing, PF resin impregnation, and hot-pressing to transform NB into an outdoor bamboo-fiber-reinforced composite (OBFRC) material with greater photostability, appropriate for outdoor buildings and decoration. The differences between the changes to the surface color, microstructure, and chemical composition of NB and OBFRC after artificial UV-accelerated aging are also investigated and compared. Finally, the mechanism dictating the photodegradation of bamboo surfaces and the enhanced photostability of the OBFRC surface is discussed. The effects of structural modification and the presence of PF resin on the photodegradation behavior of OBFRC are investigated.

2. Experimental

2.1. Raw Materials

Four-year-old moso bamboo (*Phyllostachys pubescens* Mazel) was obtained from Zhejiang Province, China. Low-molecular-weight phenol-formaldehyde (PF) resin (47.91% solid content, 35 cps viscosity, and pH 10–11) was supplied by Beijing Dynea Chemical Industry Co., Ltd, (Beijing, China).

2.2. Three-Step Process for Preparing OBFRC

The method for producing OBFRC from raw bamboo is presented in Figure 1. First, raw bamboo was processed into an oriented bamboo-fiber mat (OBFM). This conversion was performed by applying mechanical fluffing along the fiber direction, consisting of truncation in the transverse axis and dissection in the longitudinal axis [17]. Following this, a net-structure was formed by the transversely interlaced bamboo-fiber bundles, with most of the outer and inner walls being removed during this process [18]. The OBFMs were air-dried till their moisture content (MC) was approximately 6.97 wt% and immersed in 30 wt% PF resin solution for approximately 5 min at 25 °C. Subsequently, they were

drip-dried for 2 to 3 min and weighed to ensure that the final PF resin content was approximately 20 wt% [19]. The resin-impregnated OBFMs were then air-dried to obtain an MC of approximately 12 wt%. Finally, the OBFRC material was created by assembling mats symmetrically along the grain in a 300 mm × 170 mm × 15 mm mould and hot pressed (CARVER 3353, USA) at 150 °C for a time equivalent to 0.5 min/mm. To complete processing, the pressed material was incubated on a hot-plate between 30 and 40 °C. A density of 1.15 g/cm³ was obtained by adjusting the weight of the mats in the mould [9]. A peeled bamboo strip with a density of approximately 0.67 g/cm³ was used as a control. This was obtained by splitting a bamboo shoot along its longitudinal axis and peeling the bark. Both samples were sanded and conditioned at 20 °C, at a relative humidity of 65%, for 2 weeks before testing.

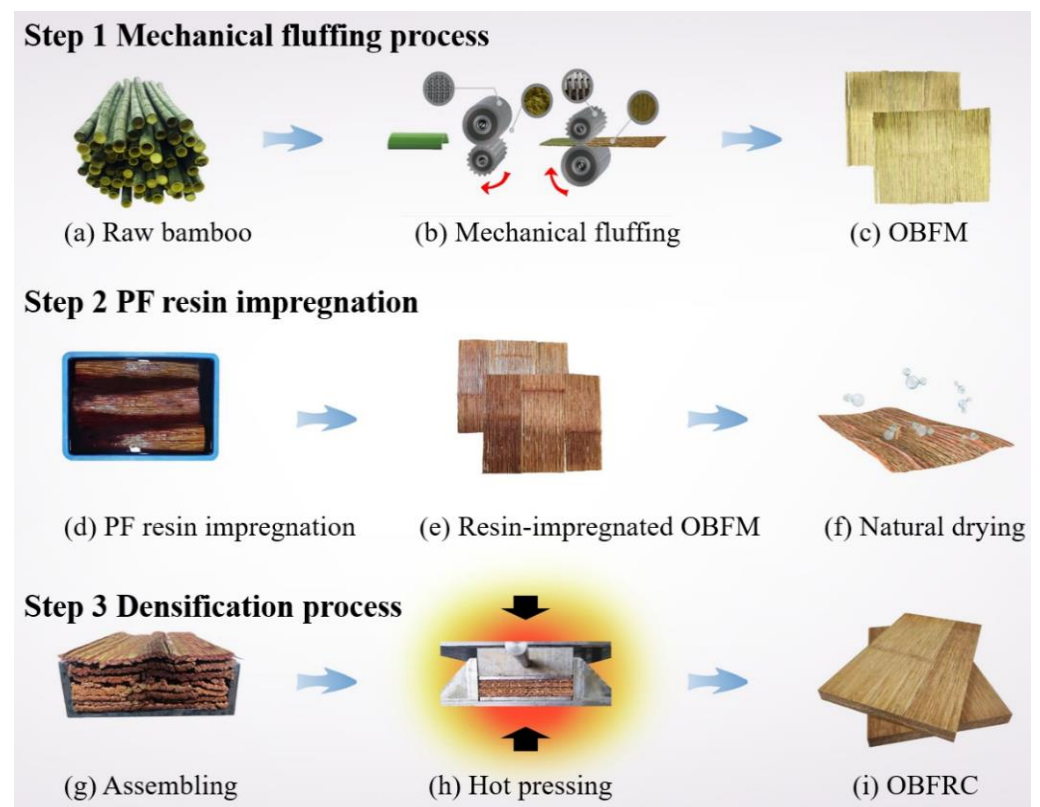


Figure 1. Three-step processing approach for creating outdoor bamboo-fiber-reinforced composite (OBFRC): Step 1: mechanical fluffing process, Step 2: phenol-formaldehyde (PF) resin impregnation, and Step 3: densification process.

2.3. Accelerated Aging Test

To model the aging process, bamboo specimens (100 mm × 25 mm × 1 mm) were exposed to light from eight fluorescent UV-visible lamps (UVA-340 lamp, H358, Q-Lab corporation, Cleveland, OH, USA) using an accelerated-UV-weathering test box (Hangzhou Nine Ring Fu Da Industrial Co., Ltd., Hangzhou, China) to simulate the total solar spectrum. For maximum simulation accuracy, the irradiance was set to 25 W/m² at 340 nm, at a black panel temperature of 63 °C [6,20].

2.4. Characterisation

The three-dimensional surface morphology and surface roughness of the specimens were examined using a digital microscopic system (VHX-6000, KEYENCE, Osaka, Japan). The internal structures of the specimens (pre-coated with Au/Pd in a vacuum sputter coater) were observed using a cold field emission scanning electron microscope (SU8020,

Hitachi, Japan; 15 kV). The surface color of each specimen was analyzed using a chroma meter (CR-400, Konica Minolta, Japan), with six measurements collected per specimen. The change in the color of a specimen was characterized using the CIELAB parameters (ΔL^* , Δa^* , Δb^* , and ΔE^*). For chemical analysis, the Fourier transform infrared attenuated total internal reflectance (FTIR-ATR) spectra were obtained directly from the specimen surface using a Nicolet iS10 FTIR spectrometer (Thermo Scientific, Waltham, MA, USA) equipped with a diamond crystal ATR accessory (Smart iTX, Thermo Scientific, Waltham, MA, USA). For each measurement, 64 scans were conducted in the 400–4000 cm^{-1} range at a resolution of 4 cm^{-1} . Similarly, X-ray photoelectron spectroscopy (XPS) was performed at 150 W using a Thermo Scientific ESCALAB 250Xi spectrophotometer (Thermo Scientific, Waltham, MA, USA) equipped with a monochromatic Al $K\alpha$ X-ray source ($h\nu = 1486.6$ eV). A nonlinear least-squares curve-fitting program (XPSPEAK software, Version 4.1) was employed for XPS spectral deconvolution.

3. Results and Discussion

3.1. Changes in Surface Appearance

A comparison between the physical appearance of the surfaces of NB and OBFRC is shown in Figure 2. Here, both surfaces are composed of vascular bundles and ground tissue cells. The difference between the texture of NB and OBFRC (Figure 2) can be attributed to the difference in the area occupied by the main constituent cells. In the natural sample, fibers account for approximately 40% of the bamboo culm by volume and 11.1% of the surface area. Conversely, fibers account for 41.65% of the surface area of OBFRC, explaining the difference in visual appearance. The presence of 20 wt% PF resin, which has a reddish-brown tint, in the OBFRC sample explains why this sample was darker than the NB sample before UV irradiation. This resin appears to have a protective effect on the OBFRC sample; although the colors of both samples were deepened after 200 h of UV irradiation, the change in color was significant with the NB sample.

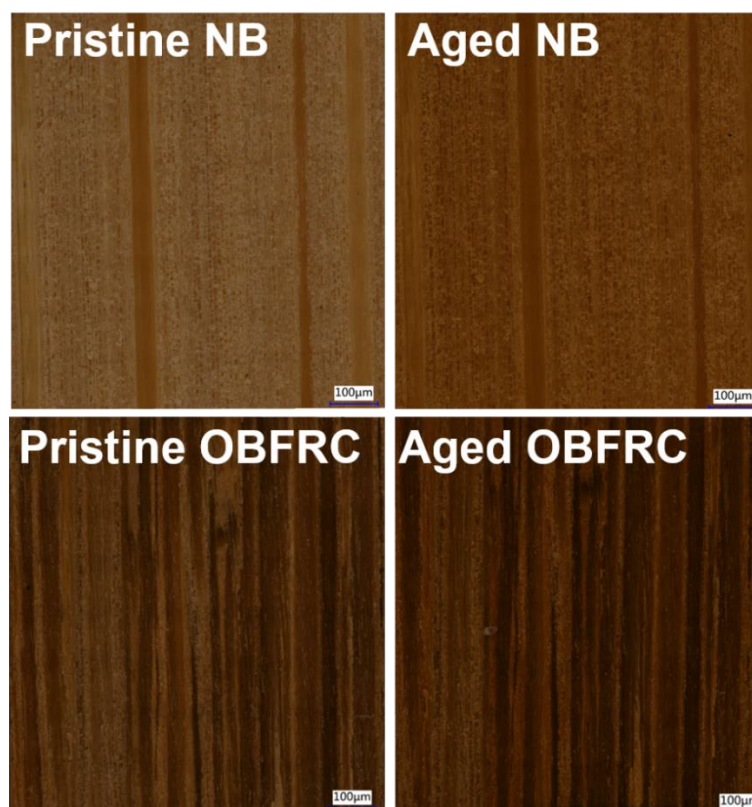


Figure 2. Visual appearance of a 5000 $\mu\text{m} \times 5000 \mu\text{m}$ region of natural bamboo (NB) and OBFRC surface before and after UV irradiation for 200 h.

Further differences in the structures of these samples that explain their difference in appearance can be observed in this image. For NB, the raised grains on the surface of the sample are vascular bundles. By contrast, for OBFRC, there are compressed ground tissue cells between the vascular bundles. This is because most vascular bundles (especially vessels) are filled with resin after impregnation [21]. Consequently, the plasticizing effect of resin on the cell wall [22,23] causes the vascular bundles to tear off irregularly in the sanding process. Moreover, in both samples, no cracks were observed after aging. However, there was an increased number of grains, and their roughness parameters also increased (Table 1), suggesting that the surface stress generated by moisture-induced dimensional changes is a key factor leading to checking and warping in the outdoor environment [24,25].

Table 1. Roughness parameters for NB and OBFRC surfaces before and after UV irradiation.

Specimens	Pristine Specimens			Aged Specimens		
	Ra	Rt	Rz	Ra	Rt	Rz
NB	2.0 (0.0)	11.3 (1.4)	18.3 (1.6)	2.3 (0.5)	16.0 (3.6)	27.2 (7.4)
OBFRC	2.0 (0.0)	11.3 (0.5)	15.3 (0.8)	2.3 (0.5)	11.8 (1.7)	16.2 (2.3)

Note: Ra = arithmetic average height, Rt = maximum height of the roughness profile, Rz = average peak to valley roughness.

3.2. Changes in Microscopic Structure

Changes to the microstructure of NB and OBFRC caused by UV irradiation were investigated using scanning electron microscopy. The internal structure of the NB sample is shown in Figure 3. Here, parenchyma cells constituting a soft ground tissue matrix that encloses the vascular bundle can be observed (Figure 3 0–1). The inner cell walls and pits on the cell walls of the parenchyma and protoxylem vessels were largely unaffected by UV irradiation (Figure 3 200–2–200–5), a fact that can be attributed to the lower degree of lignification in such cells [26,27]. However, cracks can be observed between fiber cells (Figure 3 200–6), indicating that significant damage occurred in the narrow layers of the fiber wall. This can be attributed to the accumulation of lignin in the middle lamella and lumen edge compound and at the interface between the two layers, making the lignin content higher in these regions [27]. A previous study investigating changes to the microstructure of bamboo after exposure to xenon lamps for 160 h has shown that concentric cracks form within the secondary walls of fiber cells in the cross section and that there are no significant changes in the structure of parenchyma cell walls in the tangential section [28]. However, Yu reported that, after 56 days of irradiation at a wavelength of 310 nm, many cracks appeared in the cell walls of both the parenchyma and vessel cells, specifically near the weak pits, whereas only a few cracks appeared in the void spaces of the fiber cells and the edges of the pits [29]. This difference in changes to the microstructure after UV radiation may be due to the use of artificial light sources: although short-wavelength UV can produce rapid polymer degradation, it often causes degradation by mechanisms that do not occur when materials are exposed to sunlight.

The fiber morphology of OBFRC, which is essentially unchanged from that of NB, is shown in Figure 4. Here, because of the increased fiber content per unit volume/fiber cell density, the parenchyma cells were compressed and reshaped as the space that the cell lumen occupied decreased (Figure 4 0–2). Although cracks were also observed between fiber cells in photodegraded OBFRC, these were fewer than the number of cracks observed in photodegraded NB (Figure 4 0–3). This is because the high density of OBFRC can limit light penetration and surface scattering effectively, hindering the transfer of the free radical reaction of lignin from the surface to the interior. Consequently, the photochemical reaction gradually saturates.

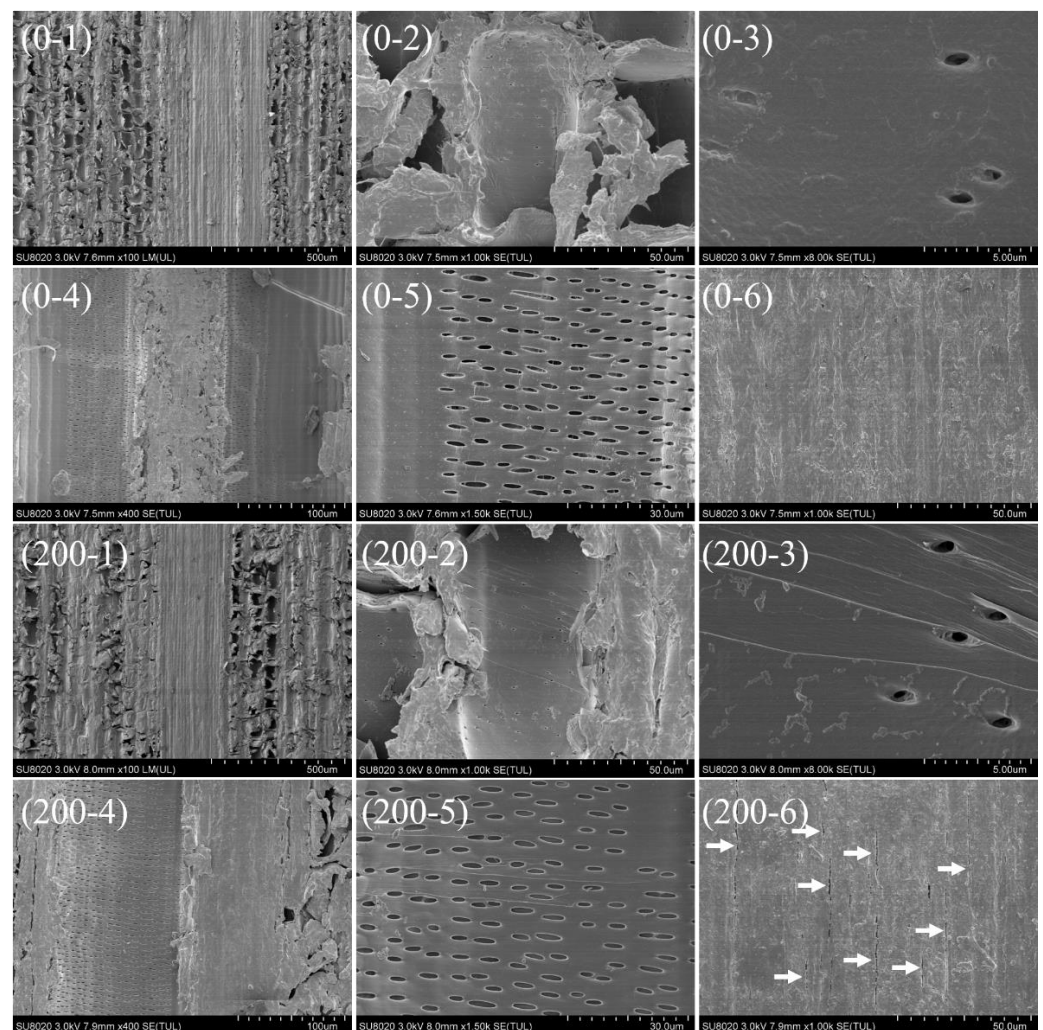


Figure 3. SEM image of a tangential section of NB (0-N) before and (200-N) after UV irradiation for 200 h. Note: N (1 to 6) denotes different regions of the tangential section.

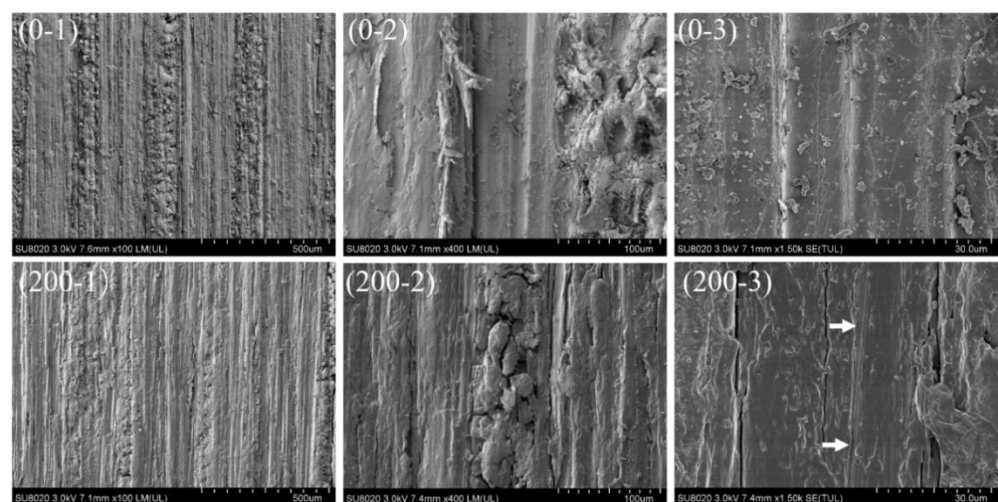


Figure 4. SEM image of a tangential section of OBFRC (0-N) before and (200-N) after UV irradiation for 200 h. Note: N (1–3) denotes different regions of the tangential section.

3.3. Color Changes

Changes to the color of NB and OBFRC surfaces owing to UV irradiation are shown in Figure 5. As previously stated, these changes are characterized using the ΔL^* , Δa^* , Δb^* , and ΔE^* parameters from the CIELAB color space. For both sets of samples, the discoloration pattern under accelerated aging conditions was consistent with that of wood [30,31]; UV irradiation made both sets of surfaces darker, as indicated by a decrease in ΔL^* with UV irradiation time (Figure 5a). In addition, the photodegraded surfaces exhibited a tendency to turn reddish and yellowish, as indicated by increases in Δa^* and Δb^* (Figure 5b,c). These changes were less drastic for OBFRC than for NB, with the former sample suppressing yellow-blue changes (Δb^* , Figure 5c) particularly well. For OBFRC, the total color change (ΔE^*) after 200 h of UV irradiation was 8.89, which is only 56.08% of ΔE^* of NB (15.85), indicating that the photostability of the former was better than that of the latter.

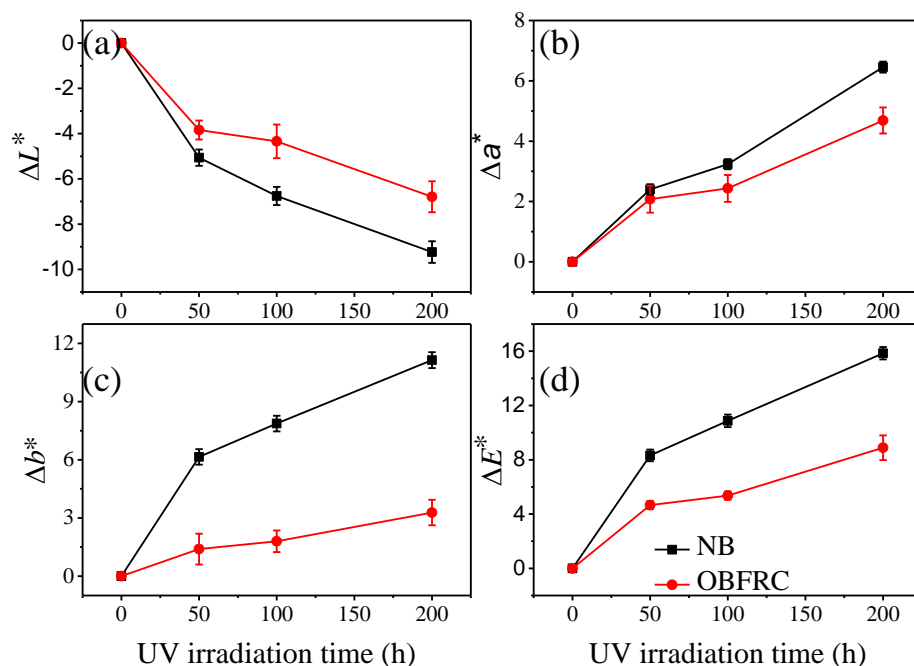


Figure 5. (a) ΔL^* , (b) Δa^* , (c) Δb^* , and (d) ΔE^* values for NB and OBFRC as functions of UV irradiation time.

According to the Beer–Lambert law, the intensity of transmitted light decreases exponentially with the depth of the lignocellulosic material [6]. The erosion rate of light on wood depends largely on its density [32,33], and, ultimately, on the thickness of its cell walls [33]. A study by Sell et al. found an approximately linear relationship between wood density (0.3–1.0 g/cm³) and erosion rate after xenon-lamp aging, for 12 types of hardwood and 6 types of softwood [33]. The cell wall of soft latewood is thicker than that of earlywood, resulting in considerably lower erosion rates. Similarly, high-density outdoor bamboo-fiber-reinforced composites (1.1–1.2 g/cm³) exhibit better surface photostability than low-density composites (0.9–1.0 g/cm³) [9]. The density of the resin-impregnated bamboo material created in this study was approximately 1.7 times that of NB, leading to an increase in the content of thick-walled fiber cells per unit volume and different degrees of parenchymal cell compression [9,18]. In addition, the PF resin completely filled bamboo cell cavities or partially adhered to their inner walls to form a thick-walled “cell wall polymer” [18,34]. These changes in structure explain the improved color stability of OBFRC.

For both sets of samples, the value of ΔE^* after UV irradiation is consistent with the rapid increase noted with 1–3-year-old bamboo aged outdoors naturally for three months [4]. With ΔE^* as the evaluation index, the photodegradation degree of NB after

200 h of irradiation at 340 nm with an intensity of 25 W/m² is equivalent to the photodegradation noted after 160 h of irradiation with a xenon lamp [2]. Both these values are lower than that obtained after three months of natural weathering outdoors [4], suggesting that further research is required into the suitability of artificial light sources in simulating the weathering effects of the outdoor natural environment on bamboo.

3.4. FTIR-ATR Analysis

FTIR-ATR spectroscopy can be used for in-situ, real-time, and non-destructive monitoring of changes to the chemical structure of the surfaces of lignocellulose materials, particularly during photodegradation and estimation of lignin content [35]. There are many well-defined peaks in the fingerprint region of the FTIR spectra (between 1800 and 800 cm⁻¹) that can quantify the variation of different functional groups present in NB and OBFRC with UV irradiation duration. Hence, prior to analysis of the spectra in Figure 6, the components of NB were assigned to characteristic FTIR bands, as listed in Table 2. Here, the 1730 cm⁻¹ band corresponds to stretching of non-conjugated C=O in hemicellulose, whereas the bands at 1595 and 1507 cm⁻¹ were assigned to aromatic skeletal vibration in lignin. Lignin is similarly responsible for the absorption peaks at 1457, approximately 1422, 1101, and approximately 833 cm⁻¹, whereas the peaks at nearly 1375, 1159, and 898 cm⁻¹ are mainly due to carbohydrates. Previous research suggested that PF resin could penetrate the secondary cell wall of wood, and cellulose could subsequently react with residual formaldehyde and/or resin oligomer [36]. In addition, during the alkaline PF curing of wood, lignin in C5 positions is partially substituted to PF moieties via methylene bridges [37]. However, because the polymeric components of the cell wall of bamboo have the same chemical structure as PF resin, the FTIR spectra of pristine NB and OBFRC have the same shape (Figure 6a,b) [2,38,39].

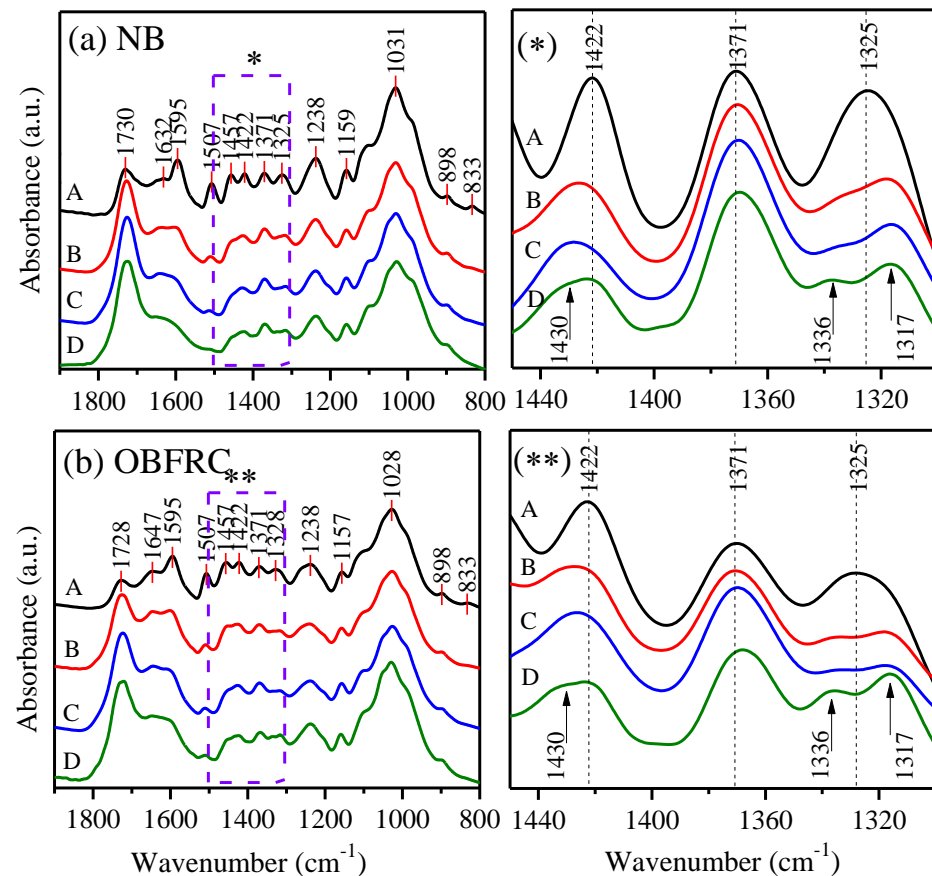


Figure 6. FTIR spectra of (a) NB and (b) OBFRC for differing periods of UV irradiation: A, 0 h; B, 50 h; C, 150 h; D, 200 h. Note: (*) and (**) are the details in the dotted box in (a,b), respectively.

Table 2. Summary of characteristic peaks in the 1800 cm^{-1} –800 cm^{-1} region of FTIR-ATR spectra for NB and OBFRC [2,28,38,39].

Wavenumber (cm^{-1})		Peak Assignment
NB	OBFRC	
1730	1728	Non-conjugated C=O in hemicellulose (xylans) and formaldehyde (PF resin)
1632	1647	Conjugated C=O in lignin
1595	1595	C=C unsaturated linkages, aromatic skeletal vibration in lignin
1507	1507	Aromatic skeletal vibration (C=C) in lignin, stronger guaiacyl element than syringyl
1457	1457	C–H deformation in lignin, and O–H in plane deformation (cellulose)
1422	1422	Aromatic skeletal vibrations (lignin), CH_2 bending vibrations in cellulose
1371	1371	C–H bending, $-\text{CH}_3$ (lignin), $-\text{CH}_2$ (carbohydrates), lignin carbohydrates complexes (LCC) bonds
1325	1328	Phenol group (cellulose)
1336	1336	O–H in plane bending (amorphous cellulose)
1317	1317	CH_2 wagging (crystalline cellulose I)
1238	1238	Syringyl ring and C–O stretch in lignin and xylan
1159	1157	C–O–C vibration in cellulose and hemicellulose
1031	1028	Aromatic C–H in plane deformation, symmetrical C–O stretching
898	898	C–H deformation in cellulose
833	833	C–H deformation in Guaiacyl units (lignin)

A comparison of the FTIR spectra from the irradiated and pristine specimen surfaces highlights significant changes due to UV irradiation. The relative content of lignin in moso bamboo is approximately 23.65% [40]. However, there was a clear decrease in the size of lignin-related peaks as irradiation time was prolonged. After UV irradiation for 50 h, the magnitude of the absorption peaks at 1595 and 1507 cm^{-1} decreased significantly, indicating that the C=C bond in the aromatic ring of lignin was broken. The size of the absorption peak at 1238 cm^{-1} , corresponding to syringyl lignin, decreased, whereas the characteristic absorption peak of the guaiacyl lignin at 833 cm^{-1} almost disappeared, indicating that guaiacyl units are more sensitive to UV than syringyl units. In addition, the size of the absorption peak at 1422 cm^{-1} was significantly reduced. The decline in the sizes of these five peaks indicates that the lignin on the surface of both NB and OBFRC experiences a fast photodegradation reaction at the beginning of UV irradiation, which is consistent with the change in the surface chemical composition of bamboo after xenon lamp irradiation [2] and natural weathering outdoors [4]. Whereas the peak at 1507 cm^{-1} had almost completely disappeared from the spectrum of NB after 200 h of irradiation, weak absorption could still be observed in the spectrum of OBFRC, indicating that the degree of photodegradation of lignin on the latter surface was less severe. This is because the increased fiber content in OBFRC limits the depth of penetration of UV light, resulting in strong resistance of the material to UV.

The intensity of the C=O-related peaks (at 1730 and 1728 cm^{-1} for natural and OBFRC, respectively) gradually increased as the duration of UV irradiation was extended. This indicates that photooxidation reactions occurred on the surfaces of both sets of samples, thereby forming new non-conjugated carbonyl compounds. For a quantitative estimate of lignin degradation and carbonyl formation, the intensity of the peak at 898 cm^{-1} , which is associated with carbohydrates, was used as an internal reference because it is unaffected by UV irradiation time [2,28]. When plotted with respect to irradiation time, an exponential decrease and increase in I_{1507}/I_{898} and $I_{1730(1728)}/I_{898}$ were observed, respectively, as shown in Figure 7a,b. Hence, the degradation of lignin and the formation of carbonyl groups was fastest in the early stage of UV irradiation; after 50 h of irradiation, I_{1507}/I_{898} decreased to 22.06% and 35.34% of its original value in NB and OBFRC, respectively. Simultaneously, $I_{1730(1728)}/I_{898}$ increased to 2.71 and 3.36 times its original value in NB and OBFRC, respectively. This result is similar to the trends noted in studies on the photodegradation of *Hevea brasiliensis*, *Pinus roxburghii* [33], and *Picea excelsa* L. [35] after xenon lamp irradiation. After 200 h of irradiation, I_{1507}/I_{898} for NB and OBFRC decreased to only 3.24% and 14.58% of their original values, respectively (Figure 7a), indicating that the retention of surface

lignin of OBFRC is higher. Conversely, $I_{1730(1728)}/I_{898}$ was lower in OBFRC than that in NB (Figure 7b) because of the pyrolysis of the temperature-sensitive hemicellulose during the hot-pressing step used for the preparation of the former material (Step 3h in Figure 1). This pyrolysis results in the cleavage of the acetyl group on the polysaccharide and a reduction in the number of ester groups [41]. Hence, after 200 h of irradiation, $I_{1730(1728)}/I_{898}$ had increased from an original value of 19.89 to 79.06 and 10.45 to 51.49 for NB and OBFRC, respectively. The lignin/carbohydrate ratio (I_{1507}/I_{898}) was subsequently plotted with respect to the carbonyl/carbohydrate peak intensity ratio ($I_{1730(1728)}/I_{898}$); a linear relationship between the two was observed for both samples, as shown in Figure 7e. This indicates that the additional carbonyl groups are products of lignin photooxidation.

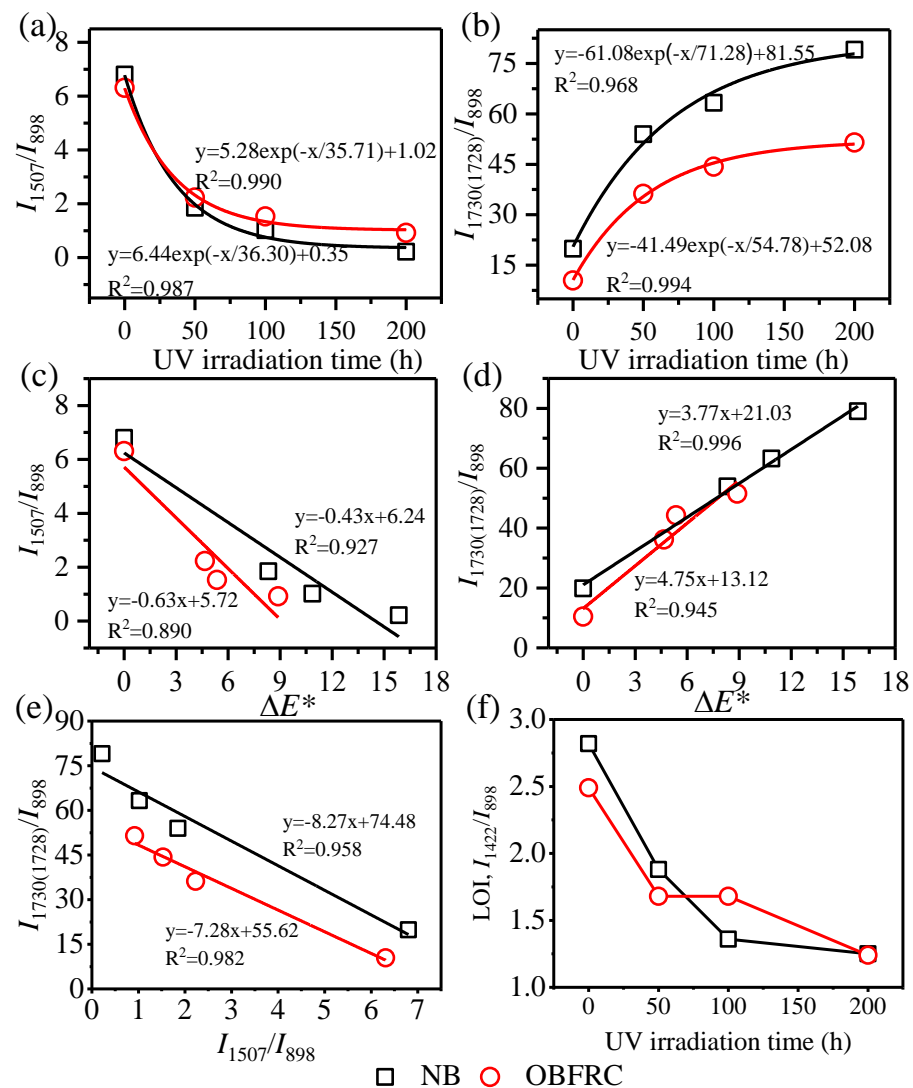


Figure 7. FTIR-ATR Analysis during photodegradation of NB and OBFRC. (a,b) Variation of lignin decay (reference peak at 1507 cm^{-1}), carbonyl group formation (reference peaks at 1730 cm^{-1} and 1728 cm^{-1}). (c,d) Correlation between color changes (ΔE^*) and decay of lignin decay, and carbonyl group formation. (e) Correlation analysis between the carbonyl formation and lignin decay. (f) Variation of crystallinity (I_{1422}/I_{898}).

The results above also indicate that photodegradation produces fewer chromophore groups with OBFRC surfaces than with NB surfaces, confirming the earlier finding that the former material is more resistant to changes in surface color. From Figure 7c,d, a linear relationship can be noted between the change in surface color (ΔE^*), lignin degradation (I_{1507}/I_{898}), and carbonyl group formation ($I_{1730(1728)}/I_{898}$) during UV irradiation. A sub-

stantial negative correlation is noted between I_{1507}/I_{898} and ΔE^* , whereas a positive correlation is noted between $I_{1730(1728)}/I_{898}$ and ΔE^* , indicating that the surface photochromism of NB and OBFRC during UV irradiation is closely related to the degradation of lignin and the resulting formation of carbonyl groups. This is consistent with previous studies on the photodegradation of bamboo and wood [2,35,42]. Here, the sensitivity of lignin to light with wavelengths shorter than 400 nm [3] can result in the formation of free radicals by its active groups and sites (including hydroxyl, carbonyl, carboxyl, aromatic, and phenolic groups) [6]. Photooxidation of the phenolic hydroxyl groups in lignin produces unstable phenolic radicals that are then transformed into *o*- and *p*-quinone structures by demethylation or side-chain cleavage [3]. These chromophoric structures are related to the photo-yellowing of the surface of the lignocellulosic material, explaining the reddening and yellowing of the NB and OBFRC surfaces during UV irradiation (Figure 5).

In contrast to lignin, cellulose and hemicellulose can only absorb ultraviolet light with wavelengths between 200 and 300 nm [6]. Since it is difficult for light in this wavelength range to reach the Earth's surface through the atmosphere, the spectrum of the UVA-340 light source used in these experiments had a limited distribution of light with $\lambda < 300$ nm. Nevertheless, Figure 7f shows that for both NB and OBFRC, the intensity of the peak at 1422 cm^{-1} gradually decreased after irradiation started, indicating that either the lignin or cellulose in the crystalline area was affected by UV. The lateral order index (LOI) is the ratio of peak areas at 1422 and 898 cm^{-1} (I_{1422}/I_{898}) of the FTIR spectra of samples, used to determine the cellulose crystallinity of the samples [24]. The LOI of both materials gradually decreased as UV irradiation time increased, reaching a final value of approximately 1.24 (Figure 7f). This behavior indicates that crystallised cellulose in these materials can be degraded, a finding that is consistent with the results of studies on the photodegradation behavior of wood [43] and heat-treated wood [24]. Simultaneously, the peak at 1422 cm^{-1} shifted to 1430 cm^{-1} , indicating either that the cellulose in the amorphous region is also susceptible to photodegradation or that the partially degraded cellulose is capable of forming new and larger crystals [5]. It has been demonstrated that, as the content of cellulose I and/or II in the crystalline region increases, the peak at 1325 cm^{-1} is gradually converted into two distinct peaks [43], corresponding to in-plane O–H bending in the amorphous region at 1336 cm^{-1} and CH_2 wagging in crystalline cellulose I at 1317 cm^{-1} [5,43,44]. The latter behavior is shown less clearly in Figure 6 * and **, indicating that, in both materials, the degradation of amorphous cellulose was more severe than the degradation of crystalline cellulose I after UV irradiation.

3.5. XPS Analysis

XPS analysis for additional investigation of the surface chemistry of bamboo photodegradation was also conducted. Since XPS cannot detect H, the most prominent elements in the spectra obtained for NB in this study were C and O from cellulose, hemicellulose, lignin, and extractives. The C peaks in the PF resin spectrum primarily originate from the benzene ring, methylene ether bond, and hydroxymethyl group in PF resin, whereas the O peaks originate from phenolic hydroxyl groups, hydroxymethyl groups, methylene quinone, and methylene ether bonds [45]. The C1s and O1s peaks in Figure 8 relate to functional groups containing carbon and oxygen, respectively. Both can be classified further according to binding energy, as C1–C4 and O1–O2, respectively. A summary of the different atomic bonding states of elemental C and O in the bamboo samples in this study is listed in Table 3.

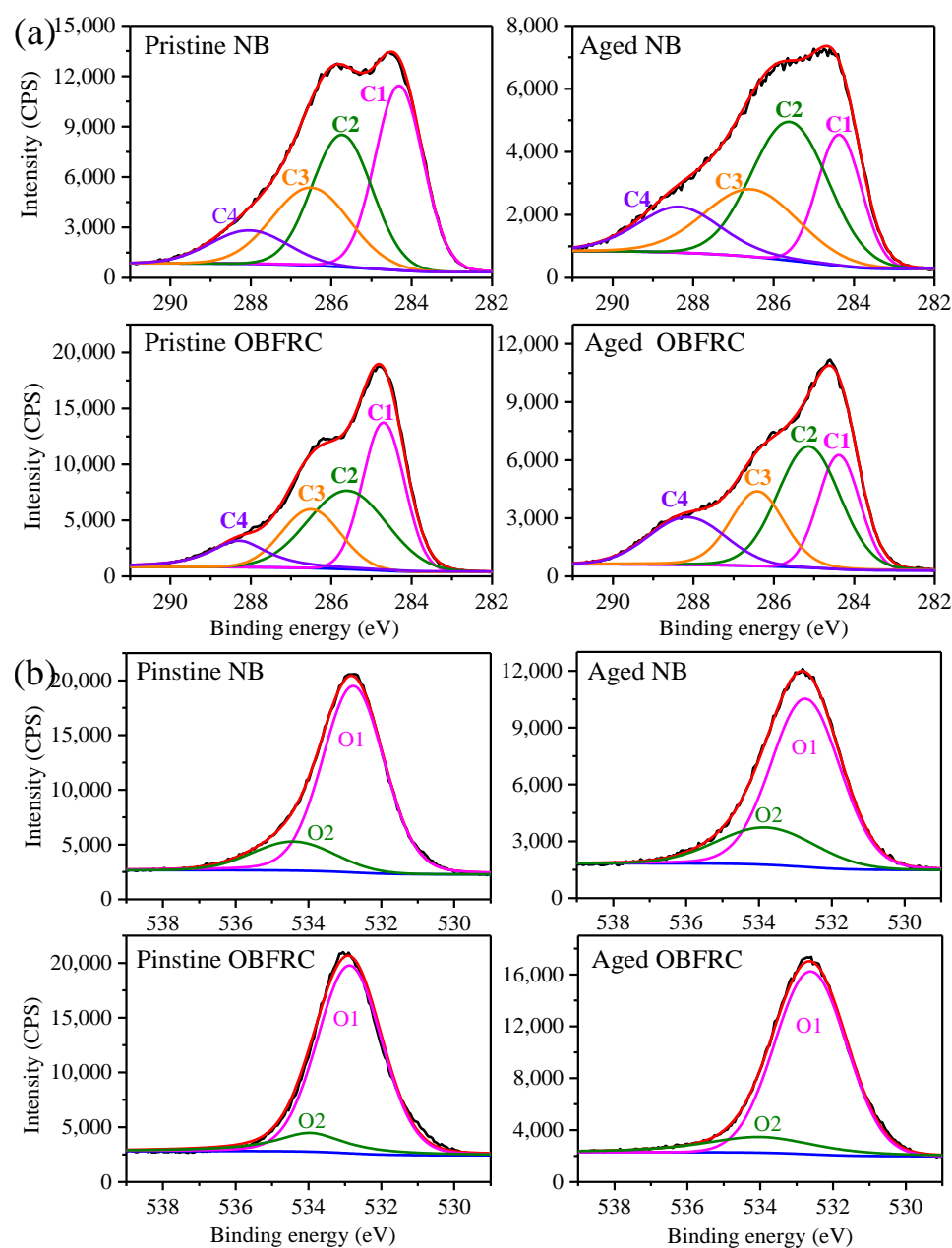


Figure 8. High-resolution XPS spectra of (a) C and (b) O peaks in NB and OBFRC before and after UV irradiation for 200 h.

Table 3. Classification of carbon and oxygen peaks in spectra for NB and phenol-formaldehyde (PF) resin [31,45,46].

Element Component	Binding Energy (eV)	Binding Type	Main Resources	
			NB	PF Resin
C				
C ₁	284.5	C–C, C–H	Lignin, fatty acids and other extracts	Benzene ring or methylene bond
C ₂	285.5	C–O	Cellulose and hemicellulose	Hydroxymethyl and phenolic hydroxyl attached to benzene ring
C ₃	286.5	O–C–O, C=O	Cellulose and hemicellulose	Active intermediate methylene quinone and methylene ether bond
C ₄	288.3	O–C=O	Hemicellulose and extracts	-
O				
O ₁	532.8	C=O	Lignin	Methylene quinone
O ₂	534.1	C–O	Cellulose and hemicellulose	Hydroxymethyl bond

The high-resolution XPS spectra of the C1s and O1s peaks measured with NB and OBFRC are shown in Figure 8a,b, respectively. Different atomic binding states were identified by deconvoluting the fitting curves, and the composition of C and O elements estimated from this deconvolution is listed in Table 4. As it has a higher C content and lower O content than NB, OBFRC has a lower oxygen to carbon (O/C) ratio than NB. This is because of the presence of 20 wt% PF resin in this material, which has an O/C ratio in the range of 0.27–0.31 [45]—lower in general than the O/C ratios of the more abundant chemical components of bamboo. The O/C ratios of cellulose and hemicellulose (xylan) were determined to be approximately 0.83 and 0.8, respectively, whereas the theoretically calculated value of the O/C ratio of lignin is approximately 0.33 [47], and the O/C ratio of the extractives is approximately 0.1 [31].

Table 4. Summary of XPS spectral parameters of NB and OBFRC before and after irradiation for 200 h.

Element Component	Pristine NB	Aged NB	Pristine OBFRC	Aged OBFRC
C	73.72	71.84	75.58	68.95
C ₁ (%)	31.03	18.04	32.04	21.54
C ₂ (%)	29.74	35.79	34.24	35.42
C ₃ (%)	25.40	26.59	20.53	22.60
C ₄ (%)	13.83	19.59	13.19	20.44
C ₁ /C ₂	1.04	0.50	0.94	0.61
C _{ox} /C _{unox}	2.22	4.54	2.12	3.64
A/B	0.77	1.24	0.90	1.27
O	26.28	28.16	24.42	31.05
O ₁ (%)	79.68	72.57	86.67	85.38
O ₂ (%)	20.32	27.43	13.32	14.62
O ₁ /O ₂	3.92	2.65	15.38	5.84
O/C	0.36	0.39	0.32	0.45

The relative content of the molecular components of bamboo can be inferred from the O/C ratio, as has been demonstrated with wood surfaces [46]. As was observed in the FTIR analysis, for both natural and OBFRC surfaces, the C content decreased after UV irradiation, and the O content increased. For NB, the O/C ratio increased from 0.36 to 0.39, whereas it increased from 0.32 to 0.45 for OBFRC. These results indicate that the lignin content on UV-irradiated surfaces decreases as the carbohydrate content increases, which is consistent with the results of the study conducted by Huang et al. [24]. The presence [48,49] and migration [31] of extractives to the surface of the material also affect its chemical composition after photodegradation. The increase in the O/C ratio of OBFRC containing PF resin was higher than that of NB because of the presence of PF resin, causing surface leaching and photooxidation in the process of PF photodegradation. In other words, PF resin acts as an antioxidant in photochemical reactions on OBFRC surfaces. This is similar to the conclusion of the study conducted by Evans et al., which showed that 30 wt% PF resin impregnation could protect the cellular structure of wood from destruction during accelerated weathering and provide limited inhibition of wood delignification [50]. The content of O on the surface of NB and OBFRC increased to differing degrees after UV irradiation (Table 4), further suggesting simultaneous photooxidation of lignin and PF resin.

After UV irradiation, the different C and O atomic binding states in both NB and OBFRC were modified similarly: there was a significant decrease in C1 content, a moderate increase in C2 and C3 content, and a significant increase in C4 content. Hence, the overall oxidation of C increased. This is because oxygen and singlet oxygen participate in surface photooxidation reactions [51], forming products with more stable chemical bonds. The differing origins of C1 and C2 indicate that the delignification of NB and OBFRC surfaces after UV irradiation is caused by the reduction or elimination of side chains—a result of the fracturing of the C-C bond [24]. Studies have shown that the C-C bond adjacent to the α -carbonyl group in lignin is broken through a Norris I type reaction. Conversely, the

ether (R-O-R') adjacent to the α -carbonyl group cannot perform the Norris I type reaction effectively. The α -carbonyl group can thus absorb light and enter an excited state. The absorbed radiation energy is subsequently transferred to the β -aryl ether bond, causing it to break and generating phenolic and carbon-based free radicals [3]. After UV irradiation, the C1 content in NB decreased by 12.99%, whereas it decreased by 10.5% in OBFRC. This indicates that the OBFRC surface was less delignified, which is consistent with the results obtained by FTIR-ATR (Figure 7).

To quantify the degree of surface oxidation, the oxygen-to-unoxxygenated carbon ratio ($C_{ox}/C_{unox} = \frac{C_2+C_3+C_4}{C_1}$) [52,53] was calculated. After UV irradiation, this ratio increased by 2.32 and 1.52 for NB and OBFRC, respectively. This indicates that the OBFRC surface experienced a lower degree of photooxidation, based on the reduced increase in hydroxyl, carbonyl, and carboxyl groups. The ratio of aromatic carbon to aliphatic carbon (C_1/C_2) reflects the lignin content in a material, based on the presence of aromatic carbons in lignin. An examination of the C_1/C_2 ratios also supports the thesis that after UV irradiation, the photodegradation of OBFRC ($\Delta C_1/C_2 = 0.43$) was less severe than the photodegradation of NB ($\Delta C_1/C_2 = 0.54$). Finally, both surfaces became more acidic after UV irradiation, as quantified by an increase to the A/B ratio ($A/B = \frac{C_2+C_4}{C_1+C_3}$) [54]. This increase in the A/B ratio was smaller for OBFRC, possibly because of the alkaline nature of the PF resin (pH 10–11) used in its preparation.

In addition to lignin, the photooxidation of PF resin contributes to an increase in O content. Hence, after UV irradiation, the increase in O content on the OBFRC surface was greater than the increase on the NB surface. The decrease in O1 content and concurrent increase in O2 content on both surfaces indicate that delignification and cellulose enrichment occur after photooxidation. Moreover, the change in O1 and O2 content was smaller for the OBFRC surface, further indicating that OBFRC experiences photooxidation less severely.

4. Conclusions

The enhancement mechanism of the surface photostability of OBFRC was primarily due to the compaction of bamboo cells and the protective effect of PF resin. Hot-pressing and compacting OBFM into OBFRC increases the relative content of thick-walled fiber cells, which compresses the parenchymal cells to varying degrees. Adding PF resin has both a structural and a chemical protective effect. Structurally, PF resin fills cell cavities or adheres to cell walls; this eventually increases the number of thick-walled cells in OBFRC substantially, thereby limiting the depth of UV light penetration and surface scattering. Chemically, after UV irradiation, the PF resin on the surface of the OBFRC is capable of photooxidation, competing with the photooxidation of lignin, and can thus play an antioxidant role that alleviates lignin degradation.

Author Contributions: Conceptualization, F.R. and N.L.; methodology, F.R.; validation, Y.J.; formal analysis, F.R.; investigation, F.R. and Y.Y.; resources, N.L.; data curation, F.R., Y.J. and Y.Y.; writing—original draft preparation, F.R.; writing—review and editing, F.R.; visualization, Y.J.; supervision, Y.Z.; project administration, W.Y. and Y.C.; funding acquisition, F.R. and N.L. All authors have read and agreed to the published version of the manuscript.

Funding: This research was funded by the Fundamental Research Funds for the Central Non-profit Research Institution of CAF (CAFYBB2018MB008), Fashion Design Talent Introduction and Training Fund project of the school of Art and Design, Zhejiang Sci-Tech University (11340031282014) and Science Foundation of Zhejiang Sci-Tech University (20082335-Y).

Data Availability Statement: The datasets generated during and/or analysed during the current study are available from the corresponding author on reasonable request.

Acknowledgments: The authors wish to thank Li Xiaoyan and Cai Wanpei for the experimental assistance.

Conflicts of Interest: The authors declare no conflict of interest.

References

1. Huang, Y.; Ji, Y.; Yu, W. Development of bamboo scrimber: A literature review. *J. Wood Sci.* **2019**, *65*, 25. [[CrossRef](#)]
2. Wang, X.; Ren, H. Comparative study of the photo-discoloration of moso bamboo (*Phyllostachys pubescens* Mazel) and two wood species. *Appl. Surf. Sci.* **2008**, *254*, 7029–7034. [[CrossRef](#)]
3. Hon, D.N.S.; Shiraishi, N. *Wood and Cellulosic Chemistry*, 2nd ed.; revised and expanded; CRC Press: Boca Raton, FL, USA, 2000; ISBN 0824700244.
4. Kim, Y.S.; Lee, K.H.; Kim, J.S. Weathering characteristics of bamboo (*Phyllostachys pubescens*) exposed to outdoors for one year. *J. Wood Sci.* **2016**, *62*, 332–338. [[CrossRef](#)]
5. Lionetto, F.; Del Sole, R.; Cannoletta, D.; Vasapollo, G.; Maffezzoli, A. Monitoring wood degradation during weathering by cellulose crystallinity. *Materials* **2012**, *5*, 1910–1922. [[CrossRef](#)]
6. Evans, P.; Mathews, M.J.C.B.; Schmalzl, K.; Ayer, S.; Kiguchi, M.; Kataoka, Y. *Chapter 14 Weathering and Surface Protection of Wood*; William Andrew Publishing: Norwich, NY, USA, 2005.
7. Zhu, R.; Zhang, Y.; Yu, W. Outdoor exposure tests of bamboo-fiber reinforced composite: Evaluation of the physical and mechanical properties after two years. *Eur. J. Wood Wood Prod.* **2015**, *73*, 275–278. [[CrossRef](#)]
8. Fei, P.; Xiong, H.; Cai, J.; Liu, C.; Yu, Y. Enhanced the weatherability of bamboo fiber-based outdoor building decoration materials by rutile nano-TiO₂. *Constr. Build. Mater.* **2016**, *114*, 307–316. [[CrossRef](#)]
9. Rao, F.; Chen, Y.; Li, N.; Zhao, X.; Bao, Y.; Wu, Z.; Ren, D.; Xu, J.; Cai, H. Preparation and characterization of outdoor bamboo-fiber-reinforced composites with different densities. *BioResources* **2017**, *12*, 6789–6811. [[CrossRef](#)]
10. Andrady, A.L.; Pandey, K.K.; Heikkilä, A.M. Interactive effects of solar UV radiation and climate change on material damage. *Photochem. Photobiol. Sci.* **2019**, *18*, 804–825. [[CrossRef](#)]
11. Hung, K.; Chen, Y.; Wu, J. Natural weathering properties of acetylated bamboo plastic composites. *Polym. Degrad. Stab.* **2012**, *97*, 1680–1685. [[CrossRef](#)]
12. Vlad, M.; Riedl, B.; Blanchet, P. Enhancing the performance of exterior waterborne coatings for wood by inorganic nanosized UV absorbers. *Prog. Org. Coat.* **2010**, *69*, 432–441. [[CrossRef](#)]
13. Rao, F.; Chen, Y.; Zhao, X.; Cai, H.; Li, N.; Bao, Y. Enhancement of bamboo surface photostability by application of clear coatings containing a combination of organic/inorganic UV absorbers. *Prog. Org. Coat.* **2018**, *124*, 314–320. [[CrossRef](#)]
14. Rao, F.; Zhang, Y.; Bao, M.; Zhang, Z.; Bao, Y.; Li, N.; Chen, Y.; Yu, W. Photostabilizing efficiency of acrylic-based bamboo exterior coatings combining benzotriazole and zinc oxide nanoparticles. *Coatings* **2019**, *9*, 533. [[CrossRef](#)]
15. Yu, H.; Pan, X.; Wang, Z.; Yang, W.; Zhang, W.; Zhuang, X. Effects of heat treatments on photoaging properties of Moso bamboo (*Phyllostachys pubescens* Mazel). *Wood Sci. Technol.* **2018**, *52*, 1671–1683. [[CrossRef](#)]
16. Plackett, D.V.; Dunningham, E.A.; Singh, A.P. Weathering of chemically modified wood. *Wood Sci. Technol.* **2000**, *34*, 151–165.
17. Yu, Y.; Huang, X.; Yu, W. A novel process to improve yield and mechanical performance of bamboo fiber reinforced composite via mechanical treatments. *Compos. Part B Eng.* **2014**, *56*, 48–53. [[CrossRef](#)]
18. Rao, F.; Ji, Y.; Li, N.; Zhang, Y.; Yu, W. Outdoor bamboo-fiber-reinforced composite: Influence of resin content on water resistance and mechanical properties. *Constr. Build. Mater.* **2020**, *261*, 120022. [[CrossRef](#)]
19. Yu, Y.; Zhu, R.; Wu, B.; Hu, Y.; Yu, W. Fabrication, material properties, and application of bamboo scrimber. *Wood Sci. Technol.* **2015**, *49*, 83–98. [[CrossRef](#)]
20. Wang, X.; Li, Y.; Wang, S.; Yu, W.; Deng, Y. Temperature-dependent mechanical properties of wood-adhesive bondline evaluated by nanoindentation. *J. Adhes.* **2017**, *93*, 640–656. [[CrossRef](#)]
21. Tomak, E.D.; Topaloglu, E.; Ay, N.; Yildiz, U.C. Effect of accelerated aging on some physical and mechanical properties of bamboo. *Wood Sci. Technol.* **2012**, *46*, 905–918. [[CrossRef](#)]
22. Shams, M.I.; Yano, H.; Endou, K. Compressive deformation of wood impregnated with low molecular weight phenol formaldehyde (PF) resin I: Effects of pressing pressure and pressure holding. *J. Wood Sci.* **2004**, *50*, 337–342. [[CrossRef](#)]
23. Gabrielli, C.P.; Kamke, F.A. Phenol-formaldehyde impregnation of densified wood for improved dimensional stability. *Wood Sci. Technol.* **2010**, *44*, 95–104. [[CrossRef](#)]
24. Huang, X.; Kocaefe, D.; Kocaefe, Y.; Boluk, Y.; Pichette, A. Study of the degradation behavior of heat-treated jack pine (*Pinus banksiana*) under artificial sunlight irradiation. *Polym. Degrad. Stab.* **2012**, *97*, 1197–1214. [[CrossRef](#)]
25. Huang, X.; Kocaefe, D.; Kocaefe, Y.; Boluk, Y.; Krause, C. Structural analysis of heat-treated birch (*Betula papyrifera*) surface during artificial weathering. *Appl. Surf. Sci.* **2013**, *264*, 117–127. [[CrossRef](#)]
26. Yang, S.; Ren, H.; Fei, B.; Jiang, Z. Lignin distribution in cell wall of bamboo culms (*Phyllostachys pubescens* and *Pseudosasa amabilis*). *Chem. Ind. For. Prod.* **2010**, *30*, 1–6.
27. Wang, X.; Ren, H.; Zhang, B.; Fei, B.; Burgert, I. Cell wall structure and formation of maturing fibers of moso bamboo (*Phyllostachys pubescens*) increase buckling resistance. *J. R. Soc. Interface* **2012**, *9*, 988–996. [[CrossRef](#)] [[PubMed](#)]
28. Wang, X.Q.; Ren, H.Q. Surface deterioration of moso bamboo (*Phyllostachys pubescens*) induced by exposure to artificial sunlight. *J. Wood Sci.* **2009**, *55*, 47–52. [[CrossRef](#)]
29. Yu, H. *Analysis on Mechanism of Bamboo UV Photo Aging*; Chinese Academy of Forestry: Beijing, China, 2015.
30. Pandey, K.K. Study of the effect of photo-irradiation on the surface chemistry of wood. *Polym. Degrad. Stab.* **2005**, *90*, 9–20. [[CrossRef](#)]

31. Wang, X.; Ren, H.; Zhao, R.; Cheng, Q.; Chen, Y. FTIR and XPS Spectroscopic studies of photodegradation of moso bamboo (*Phyllostachys Pubescens* Mazel). *Spectrosc. Spectr. Anal.* **2009**, *29*, 1864–1867.
32. Kataoka, Y.; Kiguchi, M.; Fujiwara, T.; Evans, P.D. The effects of within-species and between-species variation in wood density on the photodegradation depth profiles of sugi (*Cryptomeria japonica*) and hinoki (*Chamaecyparis obtusa*). *J. Wood Sci.* **2005**, *51*, 531–536. [[CrossRef](#)]
33. Sell, J.; Feist, W.C. Role of density in the erosion of wood during weathering. *For. Prod. J.* **1986**, *36*, 57–60.
34. Furuno, T.; Imamura, Y.; Kajita, H. The modification of wood by treatment with low molecular weight phenol-formaldehyde resin: A properties enhancement with neutralized phenolic-resin and resin penetration into wood cell walls. *Wood Sci. Technol.* **2004**, *37*, 349–361.
35. Müller, U.; Rätzsch, M.; Schwanninger, M.; Steiner, M.; Zöbl, H. Yellowing and IR-changes of spruce wood as result of UV-irradiation. *J. Photochem. Photobiol. B Biol.* **2003**, *69*, 97–105. [[CrossRef](#)]
36. Wang, X.; Deng, Y.; Li, Y.; Kjoller, K.; Roy, A.; Wang, S. In situ identification of the molecular-scale interactions of phenol-formaldehyde resin and wood cell walls using infrared nanospectroscopy. *RSC Adv.* **2016**, *6*, 76318–76324. [[CrossRef](#)]
37. Yelle, D.J.; Ralph, J. Characterizing phenol-formaldehyde adhesive cure chemistry within the wood cell wall. *Int. J. Adhes. Adhes.* **2016**, *70*, 26–36. [[CrossRef](#)]
38. Myers, G.E.; Christiansen, A.W.; Geimer, R.L.; Follensbee, R.A.; Koutsky, J.A. Phenol-formaldehyde resin curing and bonding in steam-injection pressing. I. Resin synthesis, characterization, and cure behavior. *J. Appl. Polym. Sci.* **1991**, *43*, 237–250. [[CrossRef](#)]
39. Huang, Y.H.; Fei, B.H.; Zhao, R.J. Modified mechanism of cell walls from chinese fir treated with low-molecular-weight phenol formaldehyde resin. *Spectrosc. Spectr. Anal.* **2015**, *35*, 3356–3359.
40. Yu, Y.; Huang, X.; Yu, W. High performance of bamboo-based fiber composites from long bamboo fiber bundles and phenolic resins. *J. Appl. Polym. Sci.* **2014**, *131*, 1–8. [[CrossRef](#)]
41. Tjeerdma, B.F.; Militz, H. Chemical changes in hydrothermal treated wood: FTIR analysis of combined hydrothermal and dry heat-treated wood. *Holz Roh Werkst.* **2005**, *63*, 102–111. [[CrossRef](#)]
42. Pandey, K.K.; Chandrashekar, N. Photostability of wood surfaces esterified by benzoyl chloride. *J. Appl. Polym. Sci.* **2006**, *99*, 2367–2374. [[CrossRef](#)]
43. Colom, X.; Carrillo, F.; Nogués, F.; Garriga, P. Structural analysis of photodegraded wood by means of FTIR spectroscopy. *Polym. Degrad. Stab.* **2003**, *80*, 543–549. [[CrossRef](#)]
44. Pandey, K.K. A study of chemical structure of soft and hardwood and wood polymers by FTIR spectroscopy. *J. Appl. Polym. Sci.* **1999**, *71*, 1969–1975. [[CrossRef](#)]
45. Qing, Z. *Study on Wood and Adhesive Surface/Interface Wettability Characterization and Influencing Factors*; Beijing Forestry University: Beijing, China, 2014.
46. Johansson, L. Monitoring fiber surfaces with XPS in papermaking processes. *Microchim. Acta* **2002**, *223*, 217–223. [[CrossRef](#)]
47. Kocaefe, D.; Huang, X.; Kocaefe, Y.; Boluk, Y. Quantitative characterization of chemical degradation of heat-treated wood surfaces during artificial weathering using XPS. *Surf. Interface Anal.* **2013**, *45*, 639–649. [[CrossRef](#)]
48. Pandey, K.K. A note on the influence of extractives on the photo-discoloration and photo-degradation of wood. *Polym. Degrad. Stab.* **2005**, *87*, 375–379. [[CrossRef](#)]
49. Chang, T.C.; Chang, H.T.; Wu, C.L.; Chang, S.T. Influences of extractives on the photodegradation of wood. *Polym. Degrad. Stab.* **2010**, *95*, 516–521. [[CrossRef](#)]
50. Evans, P.D.; Kraushaar, S.; Cullis, I.; Liu, C.; Sèbe, G. Photostabilization of wood using low molecular weight phenol formaldehyde resin and hindered amine light stabilizer. *Polym. Degrad. Stab.* **2013**, *98*, 158–168. [[CrossRef](#)]
51. Hon, D.N.; Products, F.; Polytechnic, V. ESCA study of oxidized wood surfaces. *J. Appl. Polym. Sci.* **1984**, *29*, 2777–2784. [[CrossRef](#)]
52. Stark, N.M.; Matuana, L.M. Surface chemistry changes of weathered HDPE/wood-flour composites studied by XPS and FTIR spectroscopy. *Polym. Degrad. Stab.* **2004**, *86*, 1–9. [[CrossRef](#)]
53. Stark, N.M.; Matuana, L.M. Characterization of weathered wood-plastic composite surfaces using FTIR spectroscopy, contact angle, and XPS. *Polym. Degrad. Stab.* **2007**, *92*, 1883–1890. [[CrossRef](#)]
54. Shen, Q.; Mikkola, P.; Rosenholm, J.B. Quantitative characterization of the subsurface acid-base properties of wood by XPS and Fowkes theory. *Colloids Surf. A Physicochem. Eng. Asp.* **1998**, *145*, 235–241. [[CrossRef](#)]